Electronic Supplementary Material (ESI) for Journal of Materials Chemistry A.
This journal is © The Royal Society of Chemistry 2020

Porous cobalt/tungsten nitride polyhedron as efficient bifunctional electrocatalysts for overall water splitting

Aiping Wu, Ying Gu, Bairui Yang, Han Wu, Haijing Yan, Yanqing Jiao, Dongxu Wang, Chungui Tian* and Honggang Fu*

Key Laboratory of Functional Inorganic Material Chemistry, Ministry of Education of China, Heilongjiang University, Harbin 150080, China

*E-mail: chunguitianhq@163.com, fuhg@vip.sina.com.

The content of ESI

1. Experimental section
2. Figure S1 The photograph of different reaction systems.
3. Figure S2 XRD pattern of CoWO precursors.
4. Figure S3 The high-magnification SEM images of CoWO precursor (a) and Co/WN-600 sample (b).
5. Figure S4 XRD pattern of powder catalysts.
6. Figure S5 XRD patterns of Co/WN-550 and Co/WN-650 samples.
7. Figure S6 SEM images of Co/WN-550.
8. Figure S7 SEM images of Co/WN-650.
9. Figure S8 XPS spectra of Co/WN-550: (a) wide scan spectrum and the high-resolution spectra of (b) Co 2p, (c) W 4f, (d) O 1s and (e) N 1s.
10. Figure S9 XPS spectra of Co/WN-650: (a) wide scan spectrum and the high-resolution spectra of (b) Co 2p, (c) W 4f, (d) O 1s and (e) N 1s.
11. Figure S10 Calculation of exchange current density of CoWO, Co/WN-550, Co/WN-600 and Co/WN-650 in 1 M KOH.
12. Figure S11 CV curves for CoWO, Co/WN-550, Co/WN-600 and Co/WN-650 in 1 M KOH with different rates from 30 to 100 mVs^{-1} in the region of 0.1-0.2 V.

13. Figure S12 Nyquist plots for CoWO and Co/WN-600 at open circuit voltage in the frequency range of 10^5-0.01 Hz.
14. Figure S13 CV curves for CoWO, Co/WN-550, Co/WN-600 and Co/WN-650 in 1 M KOH with different rates from 20 to 60 mVs^{-1} in the region of 1.15-1.25 V.
15. Figure S14 Solar power assisted water splitting device (driven by a solar panel with a voltage of 1.55 V).
16. Figure S15 The enlarged XRD patterns of Co/WN-600 after HER and OER.
17. Figure S16 The SEM images of Co/WN-600 after HER and OER.
18. Table S1 The performance of various catalysts for HER in 1 M KOH without iR compensation.
19. Table S2 The performance of various catalysts for HER in 1 M KOH with 90% iR compensation.
20. Table S3 Comparison of HER performance of Co/WN-600 with other non-noble metal electrocatalyst in 1 M KOH.
21. Table S4 The performance of various catalysts for OER in 1 M KOH without iR compensation.
22. Table S5 The performance of various catalysts for OER in 1 M KOH with 90% iR compensation.
23. Table S6 Comparison of OER performance of Co/WN-600 with other non-noble metal electrocatalyst in 1 M KOH.
24. Table S7 Comparison of overall water splitting performance of Co/WN-600 with other non-noble metal electrocatalyst in 1 M KOH.

Experimental section

Materials and chemicals

Ammonium Paratungstate [$(NH_4)_{10}H_2W_{12}O_{42}·xH_2O$] and Cobalt nitrate hexahydrate [$Co(NO_3)_2·6H_2O$] were purchased from Aladdin Chemical Reagent Co., Ltd. Ni foams was purchased from Shanghai Tanqi new material technology business department. Ethanol were obtained from Tianjin Kermel Chemical Reagent Co., Ltd. All chemicals were used without any further purification. Deionized water was used throughout the experiments.

Synthesis of porous cobalt tungsten oxynitride polyhedron on Ni foam

Firstly, Ni foam (NF) was cleaned by 2 M HNO_3 aqueous solution and deionized water with ultrasonication for 15 min in each step to remove the surface oxide layer. Secondly, one piece of treated NF (3×5 cm) was vertically placed into a 100 mL teflon autoclave with 80 mL homogenous solution containing 0.125 mmol $(NH_4)_{10}H_2W_{12}O_{42}$ • xH_2O and 1.5 mmol $Co(NO_3)_2$ • $6H_2O$. Subsequently, the teflon-lined stainless autoclave was sealed tightly and heated at 180℃ for 10 h. After it naturally cooled to room temperature, the Ni foam coated with $Co_4W_6O_{21}(OH)_2$ • $4H_2O$ precursor (named as CoWO precursor) was taken out. After sonication for 5min, the CoWO/NF precursor was washed with water and ethanol successively several times and then dried at 60℃ for 12 h. To obtain cobalt/tungsten nitride polyhedron, the as-prepared CoWO/NF precursor were treated with controlled nitridation at 600℃ for 2h with a heating rate of 5℃ min-1 in NH_3 atmosphere, followed by naturally cooling to room temperature. The product was denoted as Co/WN-600. To tune the micro-structures and composition of the cobalt/tungsten nitride polyhedron, the nitridation was also carried out at 550℃ (Co/WN-550) and 650℃ (Co/WN-650), while keeping other parameters unchanged.

Characterizations

The morphology and phase composition of as-prepared materials were studied by

scanning electron microscope (SEM, Hitachi S-4800 at an accelerating voltage of 5 kV), transmission electron microscopy (TEM, JEM-2100 at an accelerating voltage of 200 kV) and Powder X-ray diffraction instrument (Bruker D8 diffractometer using Cu Kα (λ=1.5406 Å) radiation with accelerating voltage 40 kV). The chemical state of the materials was characterized by X-ray photoelectron spectroscopy (XPS), performed on VG ESCALAB MK II using an Mg Ka (1253.6 eV) achromatic X-ray radiation.

Electrochemical measurements

All electrochemical measurements were carried out on a CHI 760E electrochemical workstation in 1 M KOH electrolyte. The electrochemical performance and characterization of as-prepared materials were tested in a three-electrode system. The as-prepared materials (Co/WN anchored on NF (1×1.5 cm)) were directly used as working electrode. Graphite rod and Hg/HgO electrode were used as the counter electrode and reference electrode, respectively. Before the electrochemical measurements, the electrolyte solutions (1 M KOH solution) were bubbled with N_2 for 1 hour to remove the dissolved gases. The activity of the electrocatalysts were evaluated by linear sweep voltammograms (LSV) tests and the polarization curves were obtained at a scan rate of 2 mV s^{-1}, which were performed after 20 cycles of cyclic voltammetry (CV) tests. In all measurements, the final potentials were calibrated to reversible hydrogen electrode (RHE) based on the Nernst equation: $E_{(RHE)} = E_{(Hg/HgO)} + 0.059 \times pH + 0.098$ V. The electrochemical double layer capacitance (C_{dl}) were obtained through cyclic voltammetry (CV) tests carried out at different scan rates in the non-faradaic potential range. The durability test was evaluated by chronoamperometry measurements at a static overpotential, during which the current variation with time was recorded. The overall water splitting measurement was carried out in a standard two-electrode system by using self-supported Co/WN polyhedron electrode as both cathode and anode in alkaline medium.

Figure S1 The photograph of different reaction systems. (1) Ammonium tungstate $[(NH_4)_{10}W_{12}O_{41}\cdot xH_2O]$ as W source; (2) Ammonium paratungstate $[(NH_4)_{10}H_2W_{12}O_{42}\cdot xH_2O]$ as W source; (3) Sodium tungstate (Na_2WO_4) as W source.

As shown in Figure S1, Ammonium tungstate (or sodium tungstate) and cobalt nitrate react at room temperature. When the two solutions of Ammonium tungstate (or sodium tungstate) and cobalt nitrate are mixed, precipitation will occur instantly, so it is difficult to obtain a well-defined structured materials. However, when ammonium paratungstate is selected as the tungsten source, a clear and transparent solution is obtained, suggesting that ammonium paratungstate can only react with cobalt nitrate under certain conditions. This result proves that the choice of tungsten source is crucial for the synthesis of CoWO precursors with a well-defined structure.

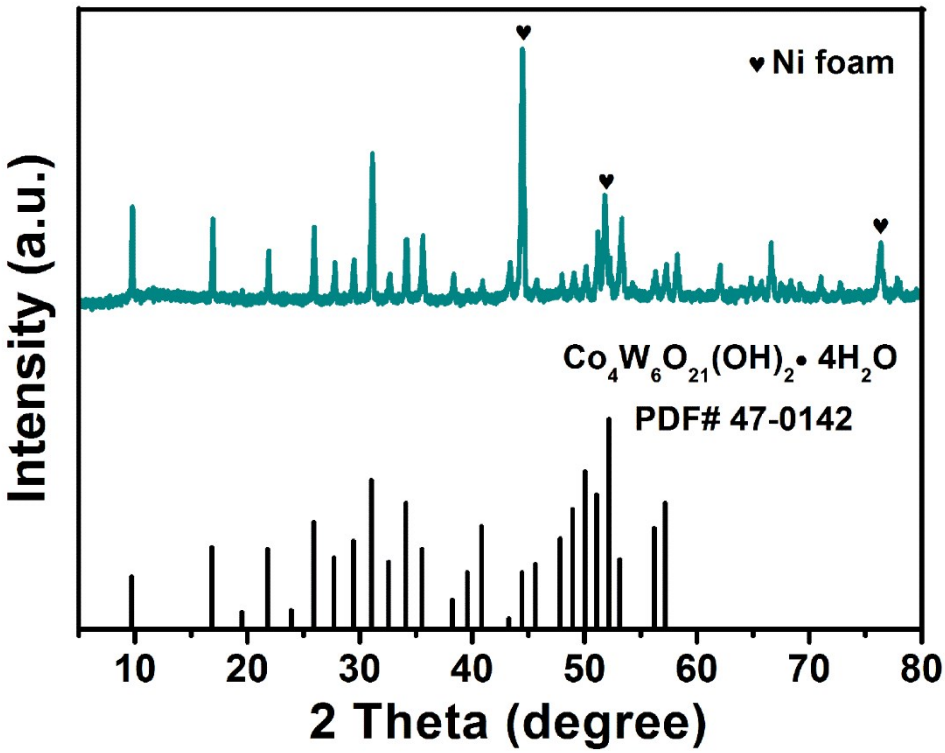

Figure S2 XRD pattern of CoWO precursors.

Figure S2 shows the XRD pattern of the sample obtained after hydrothermal reaction. As shown in Figure S2, the sample has very good crystallinity. It can be observed that except for the diffraction peaks of nickel foam, the other diffraction peaks belong to $Co_4W_6O_{21}(OH)_2 \cdot 4H_2O$ (PDF# 47-0142), suggesting that ammonium paratungstate reacts with cobalt nitrate to form a stable cobalt tungsten oxide hydroxide hydrate during the hydrothermal reaction. For convenience, the $Co_4W_6O_{21}(OH)_2 \cdot 4H_2O$ precursor was named CoWO precursor.

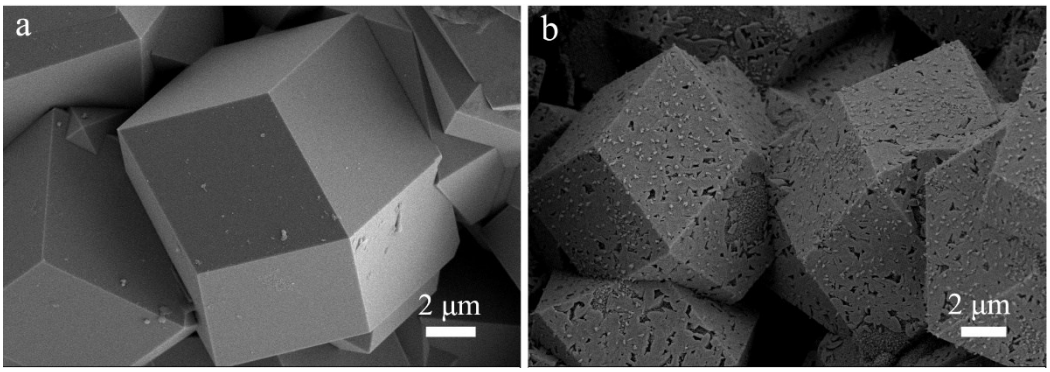

Figure S3 The high-magnification SEM images of CoWO precursor (a) and Co/WN-600 sample (b).

As displayed in Figure S3, the CoWO precursor polyhedron has a smooth surface. After controllable nitridation, the polyhedron morphology is well maintained but the volume shrinks slightly and the surface becomes rough. Importantly, it is obviously seen that there are many pores and nanoparticles generated on the surface, which may offer efficient pathway for electrolyte diffusion and expose more catalytic active sites.

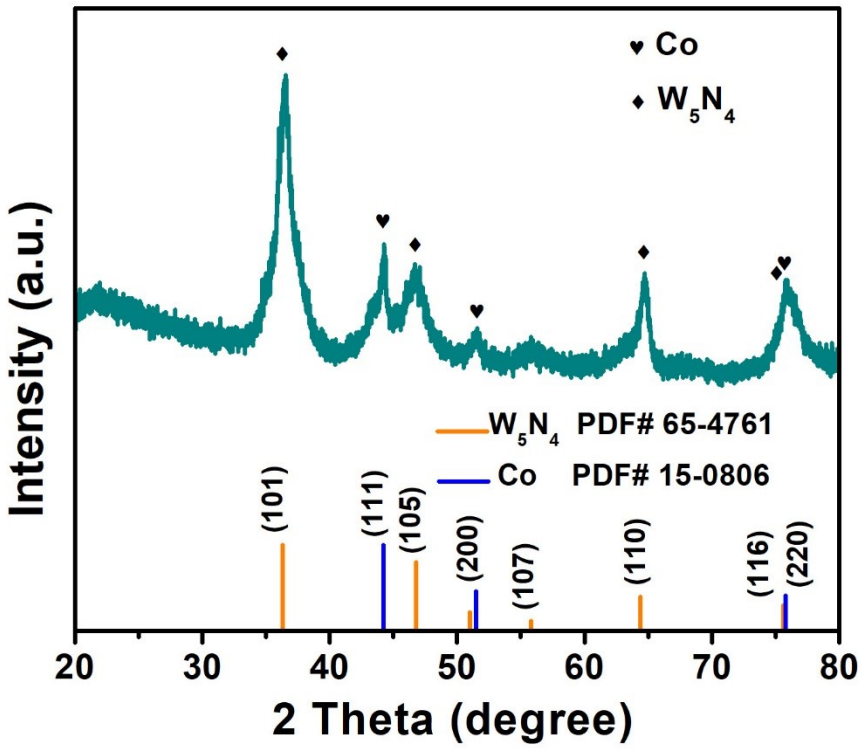

Figure S4 XRD pattern of powder catalysts.

In order to better observe the crystal structure of the Co/WN catalysts, the remaining powder samples after the hydrothermal reaction are collected and were undergone the same heat treatment as self-supporting samples. Figure S4 shows the XRD pattern of the powder catalysts. As observed in Figure S4, in addition to the diffraction peaks of W_5N_4, other diffraction peaks located at 44.2 °, 51.5 ° and 75.8 ° can be attributed to the (111), (200) and (220) planes of Co (PDF# 15-0806), indicating the cobalt species are reduced to metallic cobalt in an ammonia atmosphere.

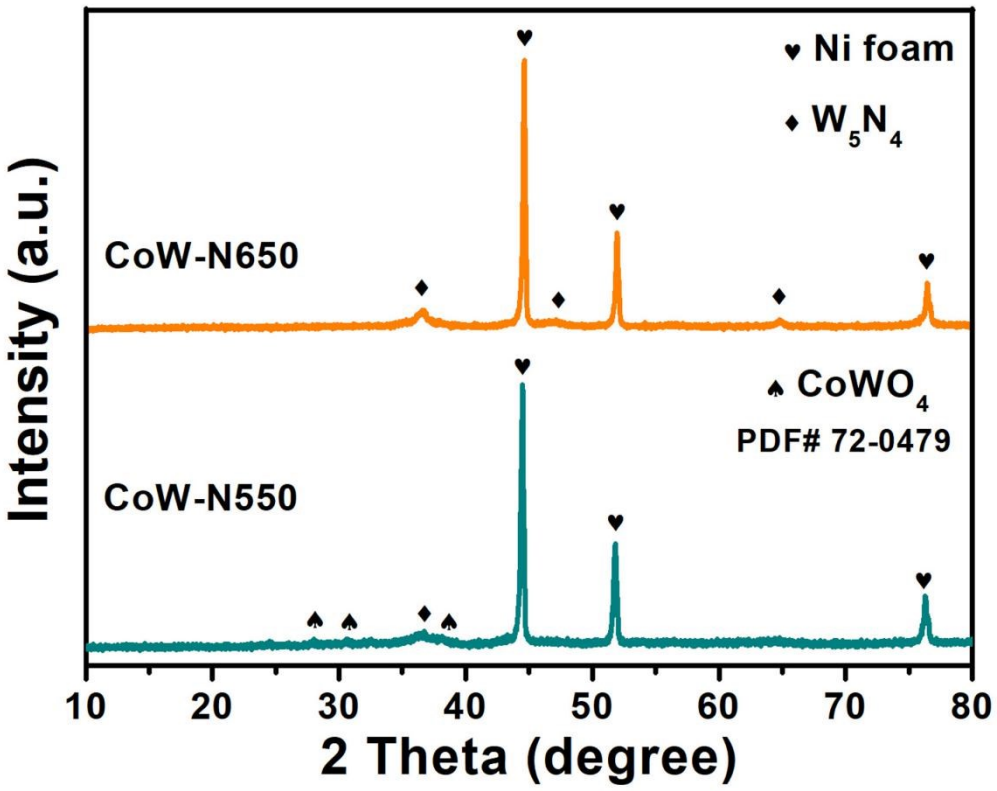

Figure S5 XRD patterns of Co/WN-550 and Co/WN-650 samples.

As shown in Figure S5, for Co/WN-550, in addition to the diffraction peaks of nickel foam and W_5N_4, other diffraction peaks can be attributed to $CoWO_4$ (PDF# 72-0479), indicating that the CoWO precursors can't be completely convert to Co/WN at a relatively low nitridation temperature. As the nitridation temperature rises to 650℃, the diffraction peak is similar to that of Co/WN-600 except that the intensity of diffraction peak becomes stronger. This result reveals that the crystallinity and the content of Co/WN can be adjusted by regulating the nitriding temperature.

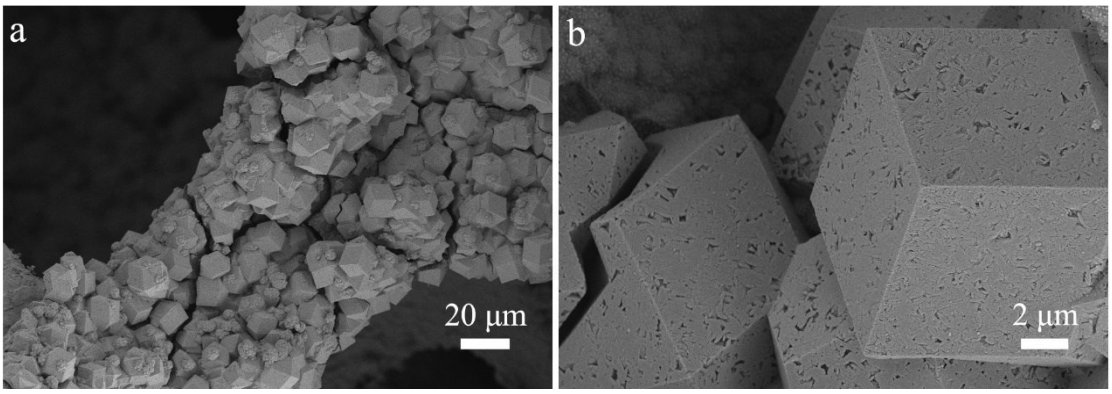

Figure S6 SEM images of Co/WN-550.

As shown in Figure S6, the morphology of Co/WN-550 is similar to the CoWO precursor, but the surface of polyhedron is very different. A large number of holes are formed due to the volume shrinkage during the high temperature nitriding process.

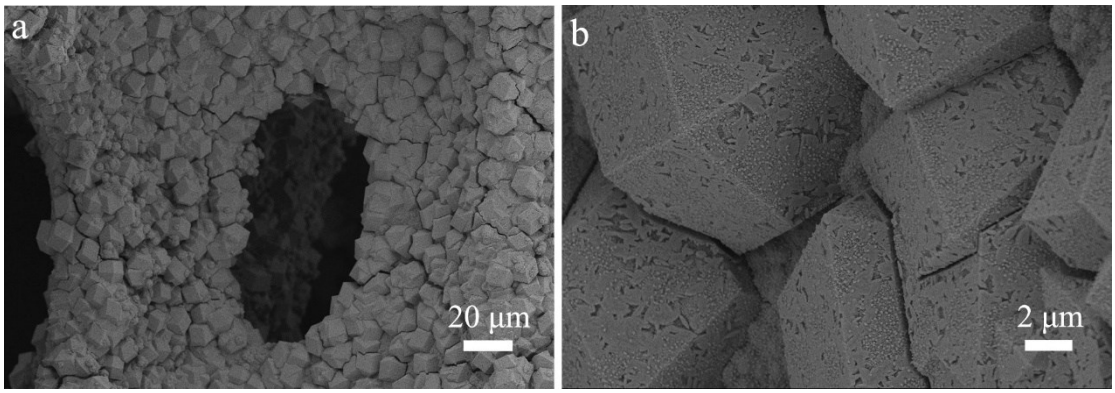

Figure S7 SEM images of Co/WN-650.

As shown in Figure S7, when rising the calcination temperature to 650℃, the polyhedron structure is still well maintained. However, the surface of the polyhedron becomes rougher and it can be obviously seen that lots of nanoparticles are loaded on the surface of the Co/WN-650, implying that the nitriding temperature is too high.

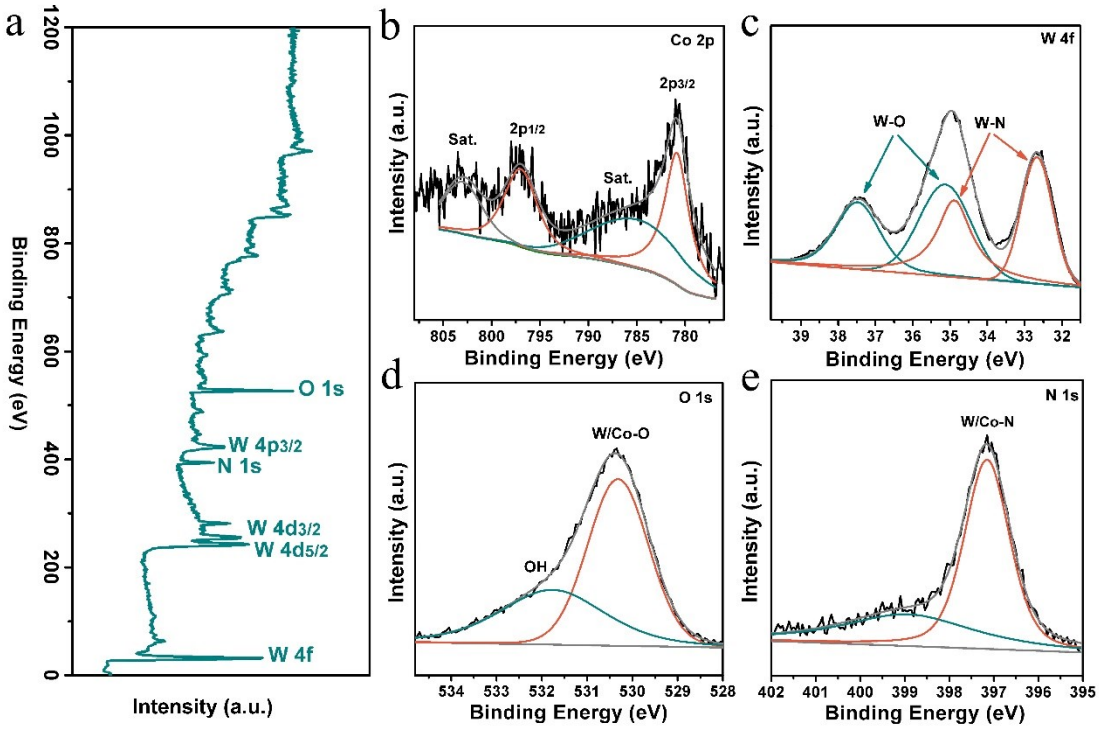

Figure S8 XPS spectra of Co/WN-550: (a) wide scan spectrum and the high-resolution spectra of (b) Co 2p, (c) W 4f, (d) O 1s and (e) N 1s.

The XPS survey spectrum of the Co/WN-550 clearly indicate the presence of W, Co, O and N elements. From the high-resolution spectra (Figure 8b-8e), it can be seen that the Co 2p spectrum is similar to that of CoWO precursor, while the XPS spectra of W 4f, O 1s and N 1s are different from that of CoWO precursor. The results indicate that the main phase of Co/WN-550 sample is $CoWO_4$. The high resolution spectrum of W 4f and N 1s prove the existence of Metal-N bonds, indicating a small amount of metal-N species were generated on the surface.

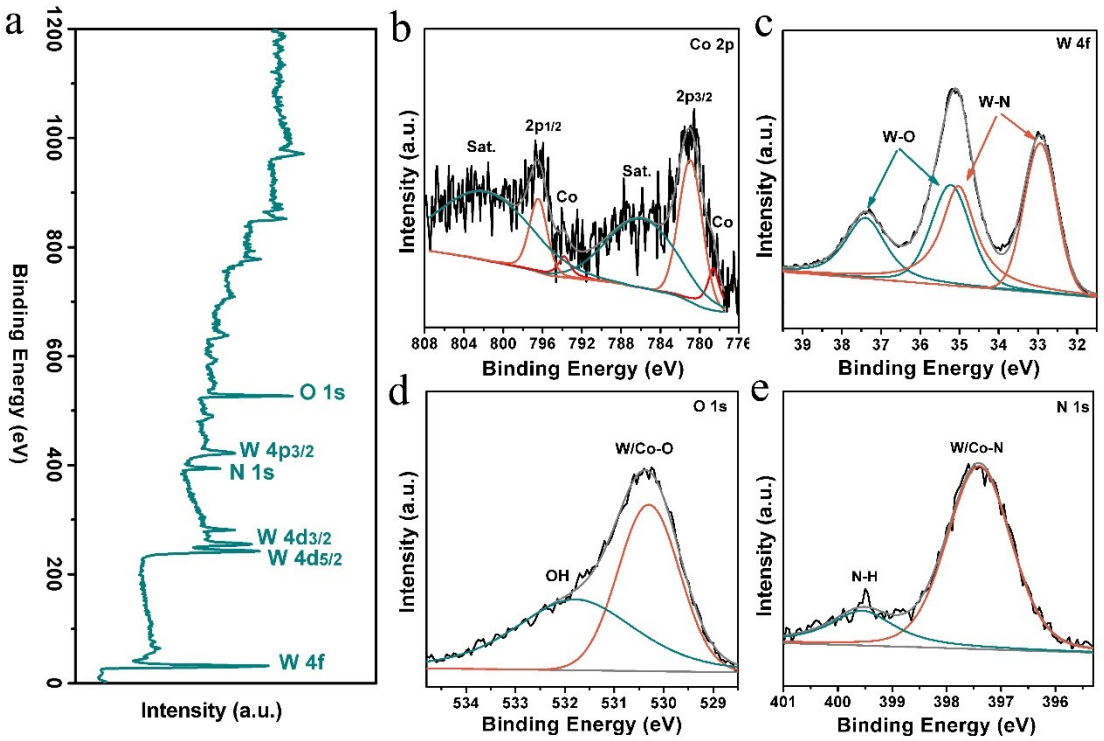

Figure S9 XPS spectra of Co/WN-650: (a) wide scan spectrum and the high-resolution spectra of (b) Co 2p, (c) W 4f, (d) O 1s and (e) N 1s.

Figure S9 shows the XPS spectra of Co/WN-650 sample. The high resolution spectra of W 4f can be divided into two pairs of distinct peaks, belonging to W-N and W-O. The XPS spectra of O 1s and N 1s are also similar to those of Co/WN-600 sample, suggesting the chemical composition of Co/WN-650 sample is similar to Co/WN-600, which is consistent with the XRD results.

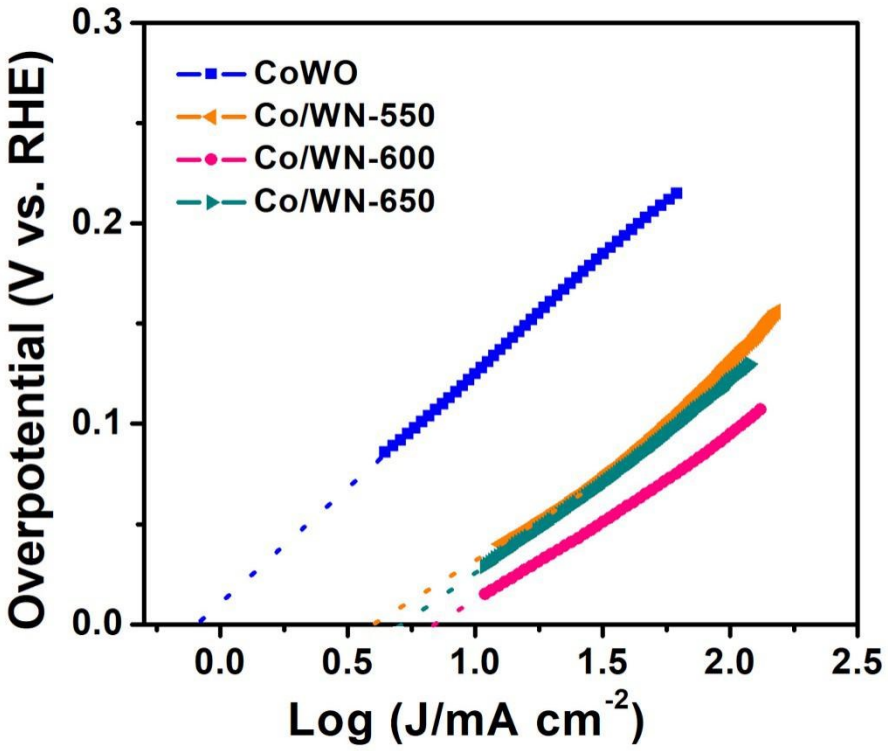

Figure S10 Calculation of exchange current density of CoWO, Co/WN-550, Co/WN-600 and Co/WN-650 in 1 M KOH.

The exchange current density (j_0) was calculated using extrapolation method. Based on Tafel equations, j_0 for Co/WN-600 sample is 6.92 mA cm^{-2}, which is higher than that of CoWO (0.84 mA cm^{-2}), Co/WN-550 (4.17 mA cm^{-2}) and Co/WN-650 (5.13 mA cm^{-2}).

The capacitive currents were measured in a potential range where no faradic processes were observed. A potential of 0.1-0.2 V at scan rates of 30-100 mV s^{-1} was utilized. The differences in the current-density variation ($\Delta j = j_a - j_c$) at the potential of 0.15 V plotted against the scan rate were fitted to estimate the electrochemical double-layer capacitances (C_{dl}), which was proportional to the ECSA.

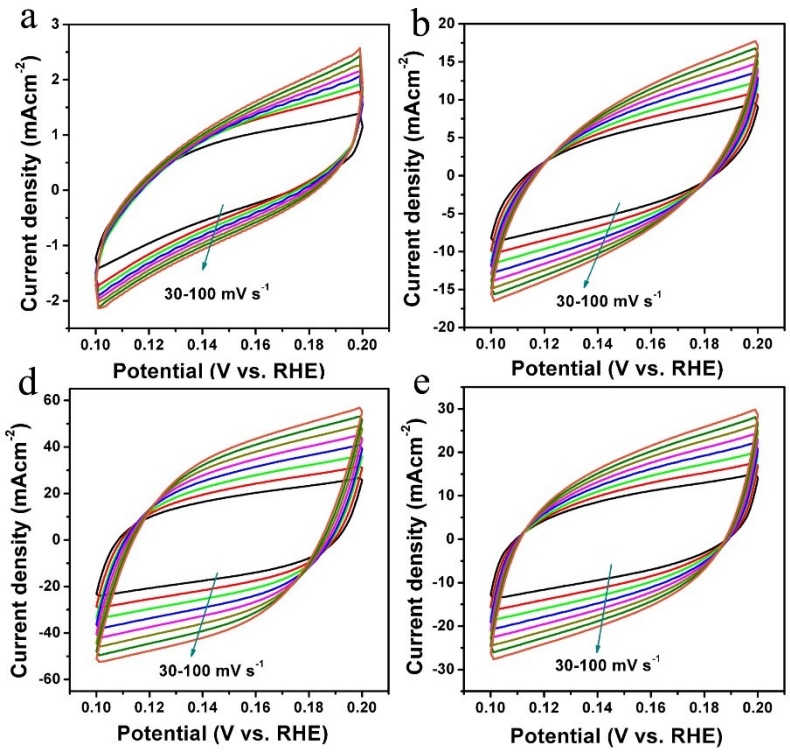

Figure S11 CV curves for CoWO, Co/WN-550, Co/WN-600 and Co/WN-650 in 1 M KOH with different rates from 30 to 100 mVs^{-1} in the region of 0.1-0.2 V.

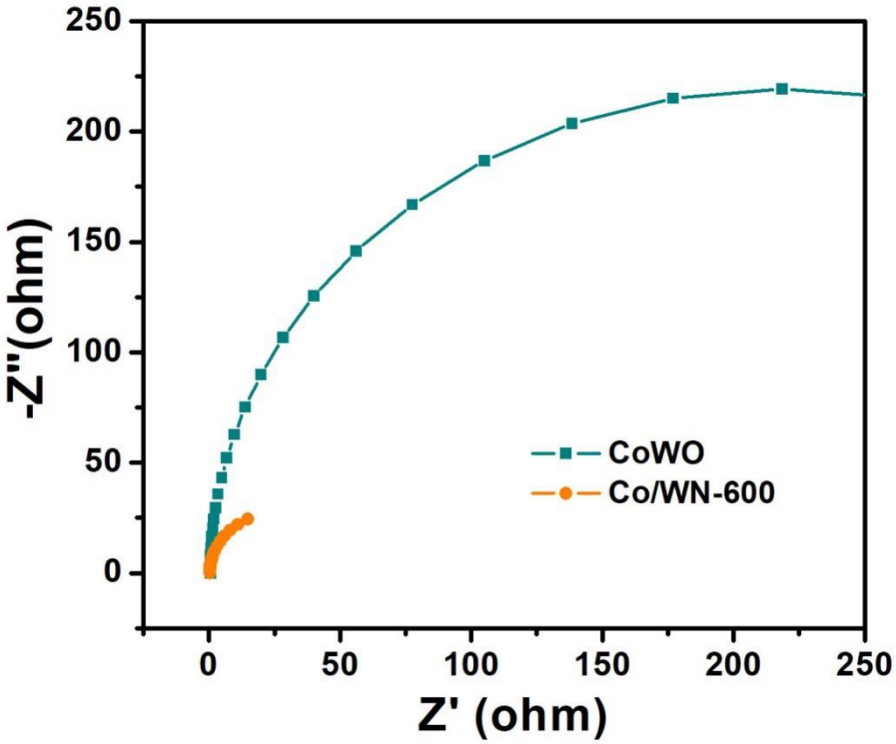

Figure S12 Nyquist plots for CoWO and Co/WN-600 at open circuit voltage in the frequency range of 10^5-0.01 Hz.

As observed from the Nyquist plots (Figure S12), the Co/WN-600 catalyst has a smaller charge transfer resistance, indicating a faster electron transfer.

.

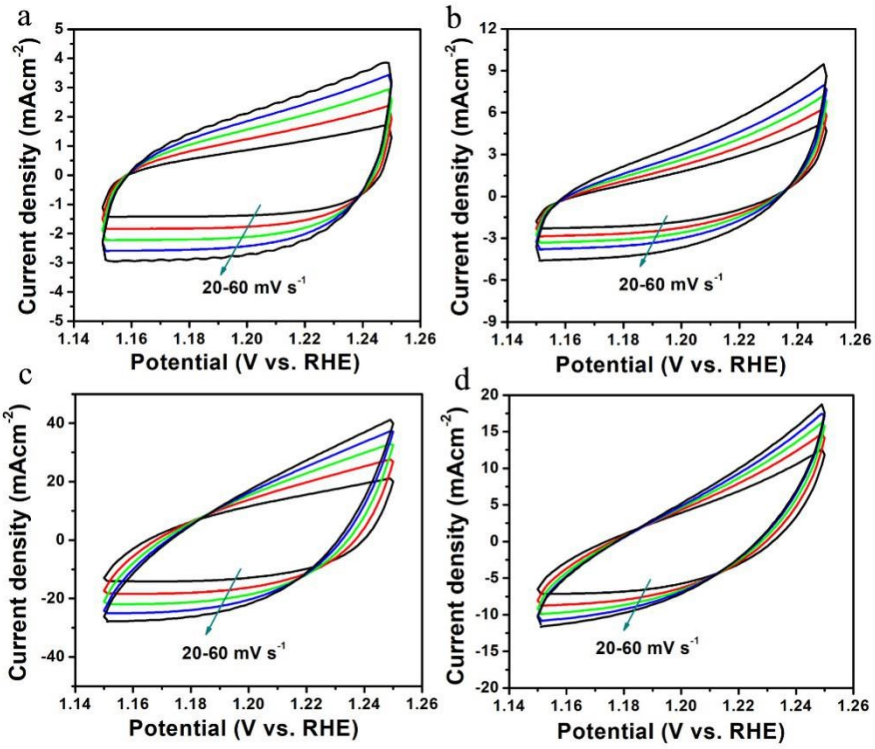

Figure S13 CV curves for CoWO, Co/WN-550, Co/WN-600 and Co/WN-650 in 1 M KOH with different rates from 20 to 60 mVs^{-1} in the region of 1.15-1.25 V.

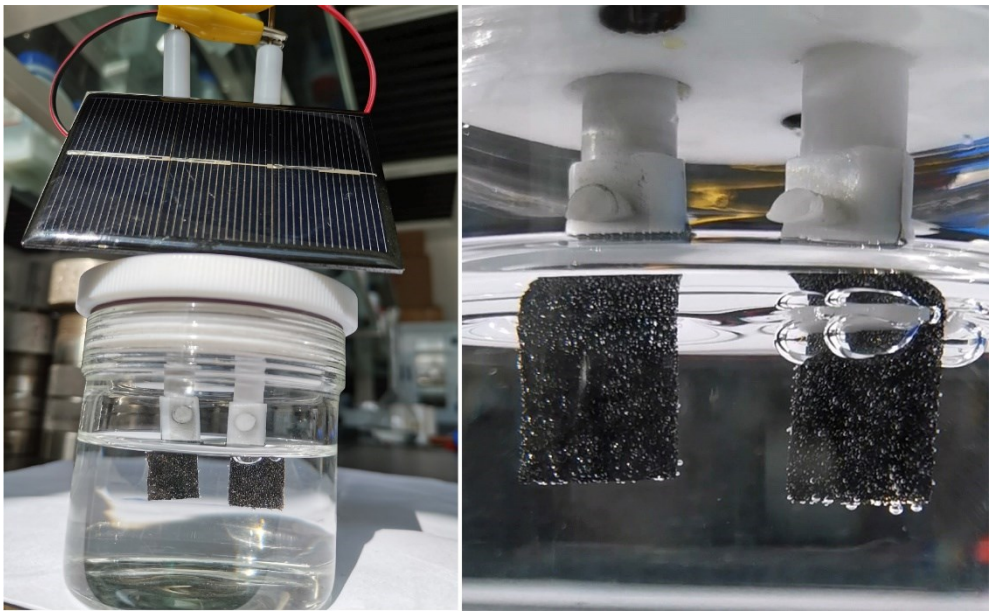

Figure S14 Solar power assisted water splitting device (driven by a solar panel with a voltage of 1.55 V).

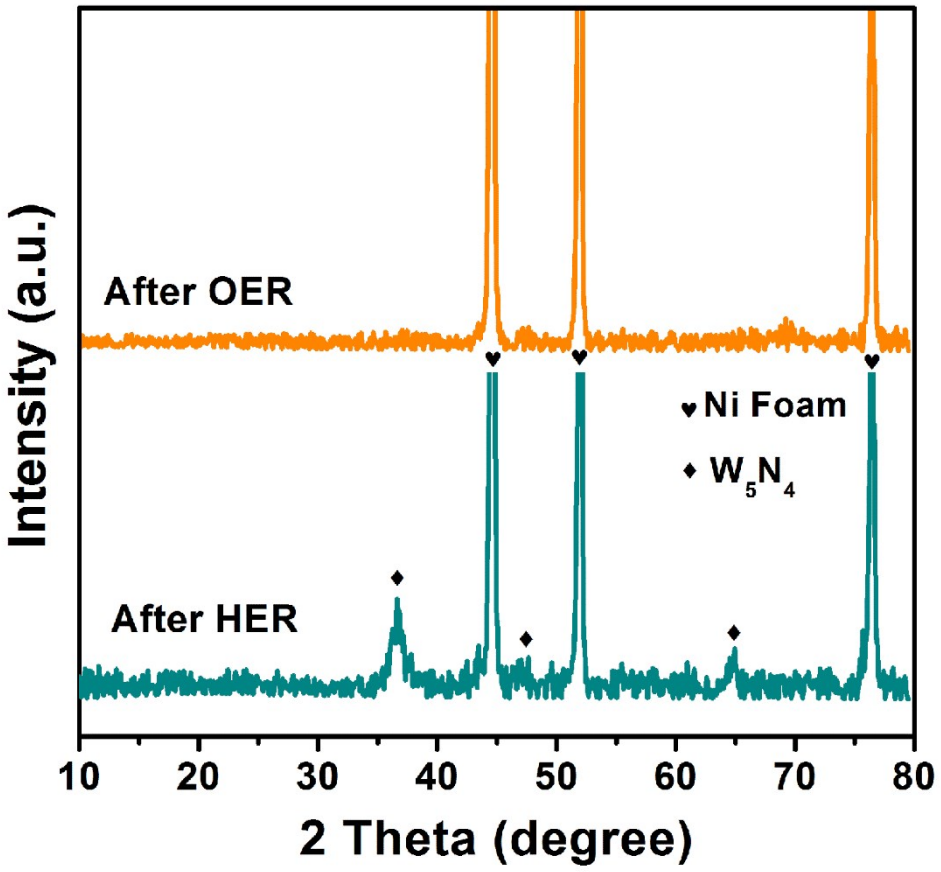

Figure S15 The enlarged XRD patterns of Co/WN-600 after HER and OER.

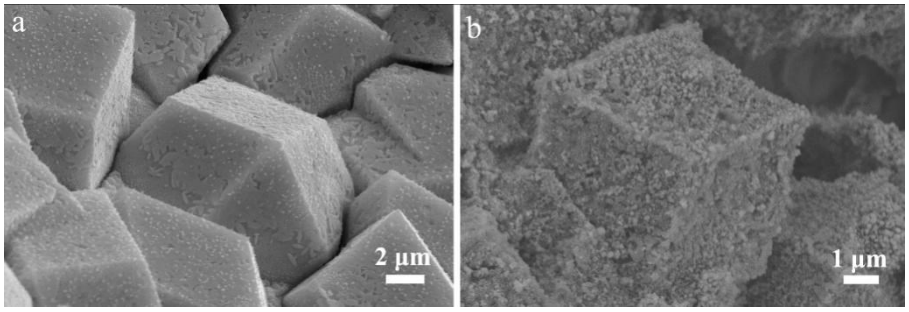

Figure S16 The SEM images of Co/WN-600 after HER and OER.

Table S1 The performance of various catalysts for HER in 1 M KOH without iR compensation.

Sample	CoWO	Co/WN-550	Co/WN-600	Co/WN-650	Pt/C
η_{10} (mV)	141	48	27	38	27
η_{100} (mV)	293	203	117	138	94
η_{200} (mV)	366	312	177	205	190

Table S2 The performance of various catalysts for HER in 1 M KOH with 90% iR compensation.

Sample	CoWO	Co/WN-550	Co/WN-600	Co/WN-650
η_{10} (mV)	126	33	12	26
η_{100} (mV)	237	132	95	122
η_{200} (mV)	265	173	126	156

Table S3 Comparison of HER performance of Co/WN-600 with other non-noble metal electrocatalyst in 1 M KOH.

Catalyst	η_{10} （mV）	Tafel slope (mV dec^{-1})	iR compensation	Reference
Co/WN-600	27	77	×	This work
S-CoWP@(S,N)-C	61	61	√	ACS Energy Lett. **2018**, 3, 1434
CoP/CoMoP	34	33	√	Nano Energy, **2020**, 68, 104332

CoMoP@C	81	55.5	√	Energy Environ. Sci., **2017**, 10, 788
$CuCo_2$-P	49.5	127.3	√	Small **2019**, 15, 1904681
$NiMo_2C$@C	181	84	×	J. Mater. Chem. A, **2017**, 5, 5000
$CoMoS_x$/NF	89	94	√	Angew. Chem. **2020**, 132, 1676
WN nanowires array	130	57.1	√	J. Mater. Chem. A, **2017**, 5, 19072
$MoS_2/CoNi_2S_4$	78	67	√	Adv. Funct. Mater. **2019**, 1908520
Cr-FeCoP	28	45	√	J. Mater. Chem. A, **2020**,8, 1184
$(Mo_2C)_x$-$(WC)_{1-x}$-QDs/NG	93	53	×	J. Mater. Chem. A, **2017**, 5, 18494
B-CoP/CNT	56	69	√	Angew.Chem. Int. Ed. **2020**, 59,4154
NiCoFePS/NF	97.8	51.8	×	Small **2019**, 1905201
Mo-NiO/Ni	50	86	√	ACS Energy Lett. **2019,** 4, 3002
$CoSe_2$@$MoSe_2$	183	87.69	√	Nanoscale, **2020**,12, 326
$(CoP)_x$-$(FeP)_{1-x}$	97	68	×	small **2017**, 1700092

Co-NiS_2NSs	80	43	√	Angew.Chem. Int. Ed. **2019**, 58,18676
NiCoP@NC NA/NF	37	53.9	×	Adv. Funct. Mater. **2019**, 1906316
W-CoP NAs/CC	94	63	√	Small **2019**, 1902613

Table S4 The performance of various catalysts for OER in 1 M KOH without iR compensation.

Sample	CoWO	Co/WN-550	Co/WN-600	Co/WN-650	RuO2
η_{10} (mV)	300	283	232	243	218
η_{100} (mV)	453	416	350	360	447
η_{200} (mV)	528	477	402	416	640

Table S5 The performance of various catalysts for OER in 1 M KOH with 90% iR compensation.

Sample	CoWO	Co/WN-550	Co/WN-600	Co/WN-650
η_{10} (mV)	272	247	190	224
η_{100} (mV)	400	348	308	322
η_{200} (mV)	433	377	327	344

Table S6 Comparison of OER performance of Co/WN-600 with other non-noble metal electrocatalyst in 1 M KOH.

Catalyst	η_{10} （mV）	Tafel slope (mV dec^{-1})	iR compensation	Reference
Co/WN-600	232	65	×	This work
$Mo_{51}Ni_{40}Fe_9$ NBs	257	51	√	ACS Catal. **2019**, 9, 1013
S-CoWP@(S,N)-C	280	68	√	ACS Energy Lett. **2018**, 3, 1434
$NiCo_2S_4$	243	58.5	×	Adv. Funct. Mater. **2019**, 1807031
tannin-NiFe	290	28	√	Angew.Chem. Int.Ed. **2019**, 58,3769
Co-NC@Mo_2C	347	61	√	Nano Energy, **2019**, 57, 746
$CoSe/MoSe_2$	262	54.9	×	J. Mater. Chem. A, **2019**,7, 3317
CoP(MoP)-$CoMoO_3$@CN	296	105	√	ACS Appl. Mater. Interfaces **2019**, 11, 6890
$Co_{1.75}Al_{1.25}O_4$ nanosheet	248	80.6	√	Small **2019**, 1804886
E-CoO_x/CF	249	50	√	Nano Energy, **2019**, 58, 778

CoOOH hollow nanospheres	275	49	√	J. Mater. Chem. A, **2019**,7, 7777
Ni_3S_4-8-NiMOF@50	257	67	√	Adv. Funct. Mater. **2019**, 1900315
Co@N-CS/N-HCP@CC	248	68	√	Adv. Energy Mater. **2019**, 1803918
Co-FeOOH/CFP	250	36	√	Small **2019**, 1901015
$FeVO_4$ nanobelts	240	37.39	√	J. Mater. Chem. A, **2019**,7, 10949
$CoMoP_2$	270	50	×	J. Mater. Chem. A, **2020**,8, 2001
Amorphous Fe–Ni–P–B–O Nanocages	236	39	√	ACS Nano **2019**, 13, 12969
NiFeSn@NiFe (Oxy)Hydroxide	260	50	√	Adv. Sci. **2020**, 1903777
Cr-CoFe LDHs/NF	238	107	√	Small **2019**, 1902373

Table S7 The performance of the recent reported electrocatalysts in alkaline solution for over overall water splitting.

Catalyst	Overpotential at 10 mA cm^{-2} (mV)		Tafel slope ($mV\ dec^{-1}$)		Overall voltage at 10 $mAcm^{-2}$(V)	Reference
	HER	OER	HER	OER		
Co/WN-600	27	232	77	65	1.51	This work
MoS_2/Ni_3S_2/Ni foam	110	218	83	88	1.56	Angew.Chem. Int. Ed., **2016**, 128, 6814
Co_6W_6C@NC	59	286	45.39	53.96	1.585	Small **2020**, 1907556
NiMo-PVP/NiFe-PVP	130	297	84	48	1.66	Adv. Energy Mater., **2017**, 1700220
Co/N-CNT/VN	63.4	240	62	53.7	1.53	Nano Energy, **2020**, 73, 104788
Ti_3C_2@mNiCoP	127	237	103	104	1.57	ACS Appl. Mater. Interfaces **2020**, 12, 16, 18570
WO_2/Ni foam	48	300	43	71	1.59	J. Mater. Chem. A, **2017**, 5, 9655
$MnCo_2O_4$@Ni_2P	57	240	89	114	1.63	Small **2020**, 2001856
Ni–Mo nitride	89	295	79	94	1.60	J. Mater. Chem. A, **2017**, 13648

($NiSe_2$/3DSNG/NF	49	-	42.77	42.89	1.59	Nanoscale, **2020**,12, 9866
$MoNi_4$/Ni foam	28	280	36	79	1.58	J. Mater. Chem. A, **2017**, 5, 2508
Mo-$NiCo_2O_4$/$Co_{5.47}N$/NF	81	310 (η_{50})	-	55.1	1.56	Small **2020**, 1906775
Co_9S_8	340	320	68	105	1.60	Adv. Funct. Mater., **2017**, 1606585
Ni-Fe-$K_{0.23}MnO_2$ CNFs-300	116	270	103.9	42.3	1.62	Small **2020,** 1905223
D-Ni_5P_4|Fe	94.5	217.3	58.4	45.7	1.59	Nanoscale, **2020**,12, 6204
Mo-Co_9S_8@C	113	200	-	95.6	1.56	Adv. Energy Mater. **2019**, 1903137
$Co(S_xSe_{1-x})_2$	122	307	85.7	67.5	1.63	Adv. Funct. Mater., **2017**, 1701008
Ar-NiCoP|V	58	246	51.7	70.4	1.55	J. Mater. Chem. A, **2019**,7, 24486
CoP NFs	136	323	56.2	49.6	1.65	ACS Catal. **2020**, 10, 412